applied sciences

MDPI

Article

Axial Compressive Behavior of Steel-Damping-Concrete Composite Wall

Chunwei Zhang [1,2], Dong An [1] and Limeng Zhu [1,2,*]

1 School of Civil Engineering, Qingdao University of Technology, Qingdao 266033, China; zhangchunwei@qut.edu.cn (C.Z.); andong@qut.edu.cn (D.A.)
2 Cooperative Innovation Center of Engineering Construction and Safety in Shandong Blue Economic Zone, Qingdao University of Technology, Qingdao 266033, China
* Correspondence: zhulimeng@qut.edu.cn; Tel.: +86-053285071328

Received: 26 August 2019; Accepted: 25 October 2019; Published: 2 November 2019

check for updates

Abstract: This paper presents a novel steel-damping-concrete (SDC) composite wall as a vertical element for high-rise buildings and nuclear power plants etc. In an SDC composite wall, a damping layer is sandwiched between the concrete core and steel plates to reduce structural response based on its damping characteristics under axial and seismic loads. To ensure that an SDC composite wall exhibits a comparable compressive resistance as a steel-concrete-steel (SCS) composite wall, two types of reinforcing approaches including steel sheets and sleeves are utilized to enhance the weakness of the damping layer on the concrete core. The compressive performance of the reinforced SDC composite wall is numerically and analytically investigated using finite element (FE) simulations by ABAQUS. The influences of several key parameters including the type of reinforcement, the thickness of the damping layer, steel plates, and concrete core, the binding bar spacing as well as the diameter of steel sheets on the compressive performance of the composite walls are investigated through numerical analyses. The results show that while only embedding the rubber interlayer in the composite wall leads to the decrease of compressive resistance of the composite wall, the steel sheets and sleeves can provide the confinement effect on concrete core efficiently and improve the compressive resistance and ductility of walls. Based on the available methods in the current design codes such as Eurocode 4, AISC-360, a theoretical model is developed to predict the ultimate compressive resistance of SDC walls. The predictions show a reasonable correlation when compared with the numerical results.

Keywords: composite wall; damping layer; reinforcement enhancement; compression behavior; finite element analysis; analytical model

1. Introduction

Steel-concrete-steel (SCS) sandwich composite structures consist of two steel plates and a central concrete core. Mechanical connectors (such as headed studs, binding bar, and J-hook) or adhesive materials (such as epoxy) are utilized in the steel-concrete interface to form an integral unit to resist external loads. Versatile applications of SCS composite structures in building cores, anti-blast and impact protective structures, road and bridge decks, shield and immersed tunnels, nuclear wall, offshore and Arctic offshore structures, liquid containment, and oil storage [1–6] are carried out due to the mechanical characteristics (such as high capacity, rigidity, blast and impact resistance, and good performance in construction efficiency and leakage prevention) of SCS composite walls.

In SCS walls, different types of materials, such as fiber-reinforced polymer (FRP) concrete, foamed concrete, lightweight concrete (LWC), ultra-lightweight cementitious composite material (ULCC), and high strength steel (HSS), are used to improve the structural performance such as compressive and shearing capacities, which are lighter weight compared with conventional walls [7–10]. To the best of the authors' knowledge, none of these studies have implemented damping materials into practice to optimize the performance and extend the application of such potential composite structures. One of these materials is rubber, which is commonly used for energy dissipation, impact resistance, and protective design of structures against blast. In order to improve the damping characteristics of composite structures, bonding an elastomeric patch or a layer (e.g., a layer with a rubber material) in particular positions of structures is one of the most common solutions. As shown in Figure 1, several studies on auto-motive and aerospace fields have been carried out on the study of damping properties of multi-coated thin-walled composite mechanical components such as plates, shells, and beams [11–13]. It can be observed that introducing layers of materials with pronounced damping properties such as high damping rubber materials [14] and viscoelastic plies constrained on their outer surfaces by stiffer layers called constrained-layer damping (CLD) treatment [15], can improve the damping properties of composite materials. Besides, there exist several studies, which investigated the effects of damping characteristics on sandwich box columns, where the damping core can be used as a viscoelastic layer (VEL), or an electro-rheological (ER) or magneto-rheological (MR) fluid core [16,17]. Recently, vibration control has become an effective method to reduce the response of civil engineering structures under horizontal load [18–20] and viscoelastic layers have been adopted particularly in the form of sandwich box columns as an alternative technological solution for efficient earthquake control (passive vibrations control) [21]. More recently, the seismic performance of reinforced concrete (RC) columns strengthened with bonded rubber plates was experimentally studied. It was observed that the equivalent damping ratio under peak load, the ductility, and the energy dissipation coefficient of RC columns attached to rubber plates were improved [22].

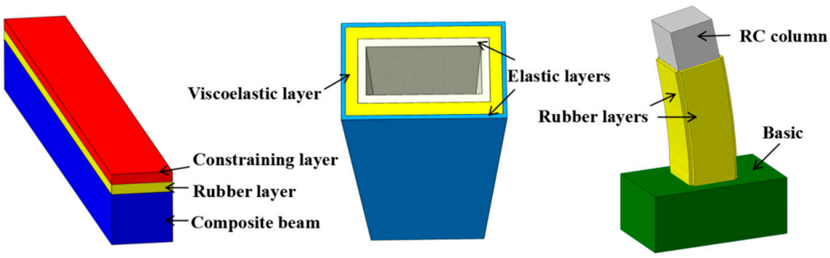

(**a**) The composite beam (**b**) The sandwich box column (**c**) The RC column with rubber plate

Figure 1. Types of composite structures with rubber layers including reinforced concrete (RC).

Rubber layers are also typical sources to increase the impact resistance of structures. For example, Kim et al. [23] and Ozturk et al. [24] improved the impact resistance of hybrid structures through the modification with epoxy resin with rubber. Then, the damping properties of hybrid structures with rubber layers under high- and low-velocity impact loads were investigated. It was found that the rubber layer could absorb the impact energy, decrease the internal damage, and increase the damage threshold in real-life applications such as laminar airfoils [25–27].

With reference to the aforementioned considerations, considering the comparability of mechanical properties and failure mode between the composite structures and laminated hybrid structures [28,29], this paper introduces a rubber layer into SCS composite wall and proposes the steel-damping-concrete (SDC) wall to improve the performance of various aspects of this versatile composite wall including the energy absorption, anti-explosion, and impact resistance.

In order to ensure the structural behavior and safety, the compressive behavior, the basic performance of vertical elements in buildings or nuclear constructions, of the composite walls is investigated in this paper. Wright [30] experimentally studied the axial behavior of the SCS sandwich walls with profiled steel sheeting. It was found that the early buckling of the external steel sheeting reduced the compression capacity of the sandwich wall. Liu et al. [31] carried out a series of experimental tests on SCS sandwich walls with short-headed studs under axial compression. Yan et al. [7] experimentally and numerically investigated the load-displacement behavior of the SCS sandwich wall with overlapped headed studs or through connectors. Huang and Liew [3,32,33] studied the axial compressive and bending behavior of SCS sandwich walls with J-hook connector, experimentally and numerically. From the aforementioned studies, the ultimate compressive resistances of SCS sandwich walls with different connectors are sufficient while the compressive ductility and the energy dissipation capacities of SCS walls are unsatisfactory. In addition, it can also be found that numerical analysis using the finite element (FE) method becomes increasingly popular and offers a cost-effective approach for carrying out pilot analysis when the research object is in the theoretical stage. The method to simulate different components and materials, the interactions among the steel plates, concrete core, and connectors, and boundary conditions in FE models of SCS sandwich walls also can be used in the SDC composite walls due to the similarities of mechanical properties and structure between the two types of composite walls [33,34].

It is important to note that only one experimental study [22] has been conducted on RC columns with bonded rubber plates but no study on SCS composite walls with rubber is reported. Moreover, the effect of the rubber interlayer in composite shear walls is not investigated. Therefore, to fill this gap, this paper introduces the rubber layer between the concrete and steel components and proposes the concept of the SDC composite wall. Compared with the conventional SCS wall, the SDC wall is characterized by better ductility and energy dissipation capacity due to the deformation of the concrete core and rubber. Binding bars working with steel sheets and sleeves are also developed as a novel type of connection between the double face plates. A validated FE model of the reinforced SDC wall, which takes into account the material and geometric nonlinearities, has been established in this research to evaluate the compressive performance of the composite walls. An extensive parametric study has been carried out to optimize the design and performance of the SDC walls. Finally, based on the available methods in the current design codes such as Eurocode 4, AISC-360 and various other literatures, a theoretical model considering the weakening effect of rubber layer on the concrete core is developed and verified herein to predict the ultimate compressive resistance of SDC walls.

2. Concepts and Theoretical Analysis of SDC Wall

2.1. The SDC Wall

Figure 2 shows the configuration of an SDC wall which consists of SCS wall components (steel plates, the concrete core, and binding bars), embedded damping (the damping layer and damping rolls), and reinforcement enhancements (steel sheets and sleeves). The bilateral steel plates and the concrete core act as the main force member of the composite wall. Whilst, binding bars are used to bond these layers of materials as integrity, similar to the SCS wall. The damping layer is sandwiched between the concrete core and external steel plates and expected to dissipate part of the input energy based on its deformation. Damping rolls are stuck to the surface of binding bars to coordinate the deformation of other components.

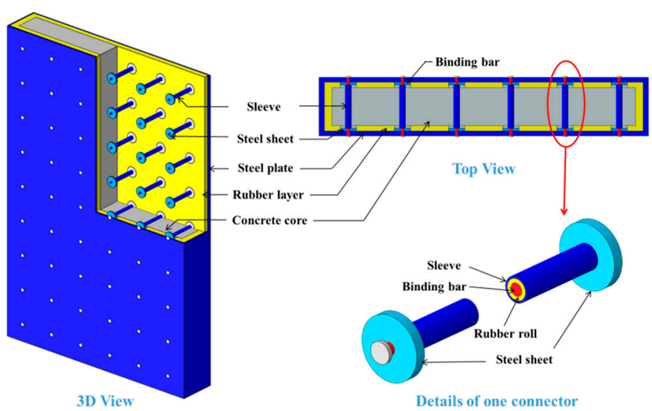

Figure 2. Configuration of the steel-damping-concrete (SDC) wall.

However, setting damping layers between the concrete core and steel plates, separates the concrete and steel plates and results in the decrease of wall compressive and shear capacity due to the loss of confinement on the concrete core as discussed in Section 4. For compensating the decreased confinement, the steel sheets and sleeves are utilized. The bilateral steel sheets are thread connected with bonding bars to enhance the confinement on the concrete core. In order to place steel sheets, circle holes in the damping layer are drilled and the thickness of the steel sheet is half of that of the damping layer which means another half of the hole in the damping layer is filled with concrete. This design produces the extra contact surfaces between the damping layer and the concrete core, which increases the interaction and integrity of the two components. Meanwhile, sleeves are stuck to the outer surface of damping rolls and designed to provide internal confinement. Compared with the SCS walls, there are three beneficial effects of the SDC walls listed as follows:

1. Embedding a damping layer in composite walls can improve its energy consumption capacity. This is because (i) when the composite wall is under compressive or seismic loading, compression and shearing deformation occurs to the damping layer sandwiched between steel plates and concrete due to their relative displacement, which can achieve energy dissipation. (ii) the damping layer can provide a space for lateral dilation for the concrete core and allow the concrete core in SDC walls to have more deformation than in SCS walls.
2. Embedding a rubber layer in the composite wall can reduce the structural response under impact load by acting as a cushion to absorb the impact energy and mitigate the internal damage.

2.2. Binding Bars with Reinforcement Enhancements

Headed studs, interlocked J-hooks, and binding bars [35], as shown in Figure 3, were invented for SCS composite walls used in high-rise buildings and nuclear building to improve the integrity of composite walls. The overlapped headed shear studs were commonly used in the steel-concrete (SC) composite structure due to its high capacity and construction efficiency. However, the tensile resistance of the overlapped headed studs profoundly depends on the confinement of concrete and this disadvantage appears more when significant cracks developed in the concrete core under extreme loads. Double J-hook connectors have equivalent structural performances and could provide a certain degree of tensile resistance without the confinement of concrete. However, high manufacturing accuracy and complexity contributed negatively to the promotion of double J-hook connectors. Meanwhile, binding bar connectors have been more popular due to the equivalent structural performance and fast installation. Cai et al. [36,37] studied the axial load behavior of square and rectangular concrete-filled steel tubular (CFT) stub columns with binding bars. Experimental results indicated that the binding bars increased the confinement of the concrete core, delayed local buckling of the tube, and improved the ductility of CFT columns. Eom et al. [38] studied the seismic behavior of the SCS sandwich wall with tie bar (bolted connections). Experiments showed that the specimens failed mainly by local buckling of the steel plates. Liu et al. [39] proposed a composite shear wall with double steel plates (CCSPW) and infilled concrete with binding bars. The results demonstrated great seismic performance of the wall. Zhu et al. [40] also experimentally studied the seismic behavior of CCSPW. It was observed that the bolt connections were failed when the horizontal loading reached a peak value which led to buckling of the steel plates. Yan et al. [7] proposed SCS sandwich walls with heads studs and through connectors. The results from the tests revealed that ultimate compressive resistance and the ductility of SCS sandwich walls significantly increased due to the existence of the connectors. However, adopting the binding bars in SCS sandwich walls mobilized additional acts in the drilling holes of the steel plates and raised the stress concentration and compromised the face integrity in the steel plates.

Considering the structural behavior and construction efficiency of the above connectors, this manuscript has developed a connection technology, which consists of a binding bar with several screw nuts, two bilateral steel sheets, and a sleeve. The binding bars are bolted to the two steel face plates of SDC walls through the holes. The bilateral steel sheets are threaded connected with the bonding bar inside of both steel plates and the sleeve covers the damping roll.

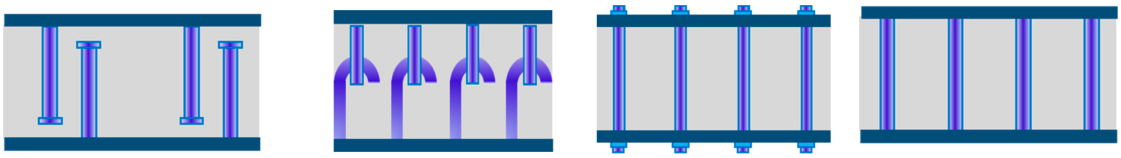

(**a**) Overlapped headed studs (**b**) Interlocked J-hooks (**c**) Binding bars (**d**) Through connectors

Figure 3. Main types of connectors used in steel-concrete-steel (SCS) composite walls.

There are four distinct features of the developed connector technology compared with the traditional connectors:

1. Adopting the binding bars avoids the manufacturing complexity of J-hooks and welding of studs.
2. The steel sheets can reduce the stress concentration effect caused by the holes on the steel plates. This is because of the internal force transmission to the vicinity of the hole can be partially shared by the steel sheets.
3. The steel sheets can also reduce the influence of the initial defects in the steel face plates. When the steel face plates are too thin to guarantee the flatness of the steel plate or the bolt spacing is too large to ensure that the concrete core, rubber layer, and steel face plates work together, steel sheets with outer screw nuts can compact the steel face plates to reduce the influence of initial concave of the steel face plates.
4. The steel sheets and sleeves can provide confinement on concrete and increase the steel content of the cross-section to improve the compressive behavior of composite walls. Figure 4 illustrates the force transmission of the SCS wall and the SDC wall with the connectors.

(**a**) SCS wall (**b**) SDC wall

Figure 4. The force transmission of the two-composite wall.

3. Model Development and Validation

3.1. General Description

The nonlinear finite element software package ABAQUS/Standard [41] is used to investigate the compressive behavior of the SDC walls taking into account both geometrical and material nonlinearities. A quarter finite element model of the SDC wall is depicted in Figure 5.

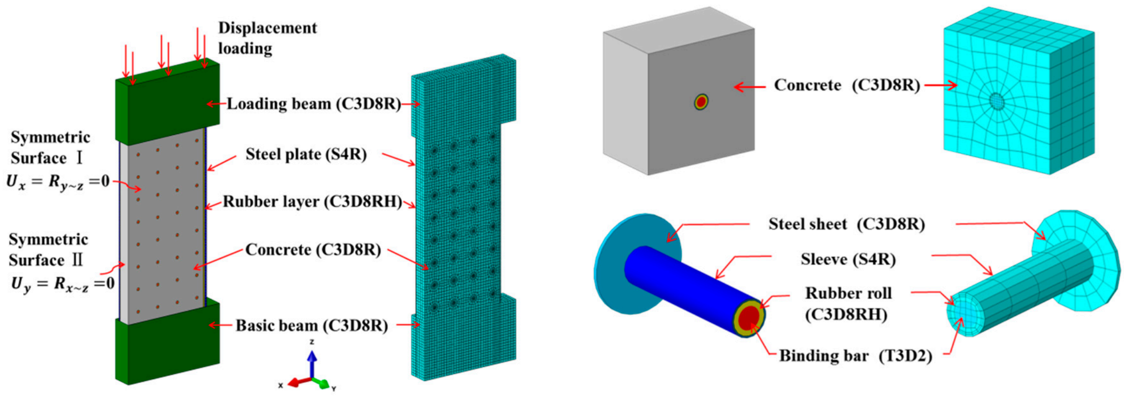

(**a**) A quarter FE model of the SDC wall (**b**) One constitutional unit of the FE model

Figure 5. Finite element (FE) models for the SDC wall.

3.2. Element, Boundary Conditions, Loading, and Interactions

Eight-node solid elements with reduced integration (C3D8R) were used to simulate the concrete core, steel sheets, the loading beam, and the foundation beam. Four-node reduced integration shell elements (S4R) were employed to model steel plates and sleeves. In addition, two-node linear three-dimensional truss elements (T3D2) were utilized to simulate the binding bars. The rubber layer and rubber roll were modeled using eight-node solid hybrid elements with reduced integration (C3D8RH) due to the incompressibility of the material. A series of mesh size sensitivity studies were carried out to make a balance between the accuracy of the FE simulations and computing efficiency. Based on the sensitivity analysis, a mesh size of 12.5 mm was selected for the elements. The coincident nodes among the elements of different components such as the steel plates, the rubber layer, and the concrete reduced the numerical cost and difficulty to obtain the converged results.

Considering the symmetric geometry and loading pattern of sandwich walls, only a quarter of the specimen FE model was built and restrained symmetrically. The displacement loading was applied to the loading beam and the bottom surface of the foundation beam was restrained against the motion in all directions.

Tie algorithm was used in the FE model to simulate the constraint among different components in sandwich walls that included the steel plate-rubber layer adhesion, the steel plate-binding bar bolted connections, and so on. A surface-to-surface contact algorithm was applied to the contact interfaces between the concrete core and the rubber layers. This algorithm adopts a "hard contact" algorithm and the "Penalty Friction contact" to simulate the behavior in the normal and tangential directions of two interacting surfaces, respectively. A friction coefficient of 0.6 was defined by a sensitivity analysis, which showed that the friction coefficient leads to a limited difference between ultimate compressive resistance and ductility with values less than 5%.

3.3. Material Constitutive Models

3.3.1. Concrete Constitutive Models

To simulate the concrete core, a concrete damage plasticity (CDP) model was utilized in which the compressive and tensile behaviors of the concrete is modeled. In this paper, these behaviors were modeled based on the characteristics defined in GB 50010-2010 [42] as follows:

$$\sigma = (1 - d_c)E_c\varepsilon \tag{1}$$

$$d_c = \begin{cases} 1 - \frac{\rho_c n}{n-1+x^n}, & x \le 1 \\ 1 - \frac{\rho_c}{(x-1)^2+x}, & x > 1 \end{cases} \tag{2}$$

where $\rho_c = \frac{f_c}{E_c \varepsilon_c}$; $n = \frac{E_c \varepsilon_c}{E_c \varepsilon_c - f_c}$; $x = \frac{\varepsilon}{\varepsilon_c}$; σ denotes the compressive stress of the concrete; ε is the compressive strain of the concrete; d_c is the axial compressive damage parameter; f_c is the ultimate compressive strength of the concrete; and ε_c is the compressive strain corresponding to f_c.

$$\sigma = (1 - d_t) E_c \varepsilon \tag{3}$$

$$d_c = \begin{cases} 1 - \rho_t \left[1.2 - 02x^5\right], & x \le 1 \\ 1 - \frac{\rho_t}{\alpha_t (x-1)^{1.7} + x}, & x > 1 \end{cases} \tag{4}$$

where $\rho_t = \frac{f_t}{E_c \varepsilon_t}$; $x = \frac{\varepsilon}{\varepsilon_t}$; σ denotes the tensile stress of the concrete; ε denotes the tensile strain of the concrete; d_t denotes the axial tensile damage parameter; f_t denotes the ultimate tensile strength of the concrete; ε_t denotes the tensile strain corresponding to f_t; and α_t denotes the axial tensile regression parameter.

In CDP models above, as shown in Figure 6, unidirectional stress-strain curves are required and the dilation angle is utilized to describe the friction properties and shear behavior of concrete at confining pressure. According to the reference [43], the dilation angle can be defined as 30°. An additional sensitivity analysis was carried out and a limited difference of ultimate compressive resistance and ductility was found with values less than 5%. Also, a small value for the viscosity parameter $\kappa = 0.0001$ was used to improve the convergence rate in the concrete following the suggestion from Huang and Liew [2].

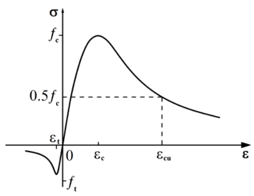

Figure 6. Stress-strain relationship for concrete.

3.3.2. Steel Constitutive Models

In this study, the steel material adopts a nonlinear isotropic hardening model that utilizes the Von-Mises yield surface to describe the isotropic yielding. According to the suggestion by Liu et al [3], as shown in Figure 7, simplified four-stage quadric flow plastic model was used for simulating the behavior of the steel face plates, the steel side plates, and the sleeves as follows:

$$\sigma = \begin{cases} E_a \varepsilon, & (0 \le \varepsilon < \varepsilon_{ay}) \\ f_{ay} & (\varepsilon_{ay} < \varepsilon \le 10\varepsilon_{ay}) \\ f_{ay} + \frac{f_{au} - f_{ay}}{90\varepsilon_{ay}} & (10\varepsilon_{ay} < \varepsilon \le 100\varepsilon_{ay}) \\ f_{au} & (\varepsilon > 100\varepsilon_{ay}) \end{cases} \tag{5}$$

where f_{ay} is the yield stress of the steel; ε_{ay} represents the yield strain of the steel; $\varepsilon_{ay} = f_{ay}/E_a$; E_a is Young's modulus of the steel; and $f_{au} = 1.6 f_{ay}$ is the ultimate tensile stress of the steel.

(**a**) Steel plates, steel sheets, and sleeves (**b**) Binding bars

Figure 7. Stress-strain relationship for steel.

And a bi-linear stress-strain curve was utilized for simulating the behavior of the binding bar:

$$\sigma = \begin{cases} E_b \varepsilon, & (0 \leq \varepsilon \leq \varepsilon_y) \\ f_y + 0.01E_b(\varepsilon - \varepsilon_y) & (\varepsilon > \varepsilon_y) \end{cases} \tag{6}$$

where f_y is the yield stress of binding bars; ε_y represents the yield strain of binding bars; $\varepsilon_y = f_y / E_s$; and E_s is Young's modulus of binding bars.

3.3.3. Damping Interlayer Constitutive Models

Mooney-Rivlin model was adopted to simulate the rubber. In the Mooney-Rivlin model, the strain energy density function W is a linear combination of two invariants of the left Cauchy-Green deformation tensor. The strain energy density function for an incompressible Mooney-Rivlin material is as follows:

$$W = C_1(\bar{I}_1 - 3) + C_2(\bar{I}_2 - 3) \tag{7}$$

where C_1 and C_2 are empirically determined material constants, and $\bar{I}_1$ and $\bar{I}_2$ are the first and the second invariant of the deviatoric component of the left Cauchy-Green deformation tensor.

It has been confirmed that material constants of the Mooney-Rivlin model are related to the linear elastic shear modulus G, which can be calculated as follows:

$$G = 2(C_1 + C_2) \tag{8}$$

It can be found from the strain contours of the FE model of the SDC wall (in Section 4) that during the axial deformation, the maximum strain of rubber parts (the rubber layer and rubber rolls) is less than 80%. According to the reference [44], compared with other constitutive models for rubber (such as the Neo-Hookean model and Ogden model), Mooney-Rovlin model is more appropriate for modeling the behavior of high damping rubber (such as chloroprene rubber) in small strain ranges.

3.4. *Validation of The Finite Element Model*

Four experimental SCS walls with various spacing of connectors carried out in reference [31], were selected to assess the reliability of the FE models developed in this study. The geometry, material details, and test results are given in Table 1.

Table 1. Dimension and material properties of the SCS walls in reference.

Specimen	Dimension (mm^3)	t_c (mm)	t_s (mm)	Spacing of Connectors (mm)	Concrete	Steel			P_u (kN)
					f_{cu} (MPa)	f_y (MPa)	f_u (MPa)	ε_y (%)	
DSW-1	700 × 166 × 800	160	3	150	52.4	370	490	0.18	6270
DSW-2				100	46.8				6390
DSW-3				75	52.4				6700
DSW-4				35	46.8				7780

*t_c = thickness of concrete core; t_s = thickness of steel plate; f_{cu} denotes the compressive stress of concrete cube; f_y is the yield stress of steel plates, f_u is the ultimate tensile stress of steel plates; ε_y represents the yield strain of steel plates; and P_u is the ultimate compressive resistance of composite walls.

The validation of the FE model for the composite walls under axial loading is presented in Figure 8. It is seen that the FE models can reasonably predict the ultimate compressive resistance and the initial stiffness of DSW 1–3. In terms of initial stiffness, the FE results are slightly conservative compared to the experimental test results and the compressive resistance of the four groups of test data increased from 200 kN. This may be justified by the instability of the force sensor of the loading device when the reaction force is marginal. In addition, the initial stiffness of DSW-4 in the FE model was lower than that in the test data due to the lower initial displacement rather than the actual displacements measured by the loading device and loading beam at the commencement of the experiment [45]. Figure 9 shows the comparison of the primary failure modes between those from the FE simulations and the test results. The local buckling of the steel plate can be captured for DSW-3 but the deviation of the distribution of buckling are also found. This is because the position of the maximum out-of-plane displacement of steel plates cannot be simulated accurately by the FE model due to the uncertainty of the initial imperfection of steel face plates. As shown in Figure 9c,d, the lateral deformation occurs on the steel plate and the tension fracture in the weld between the steel face plate and the side plate. And the maximum out-of-plane displacement of the steel side plate is 1.1 mm which agrees well with the numerical results [45].

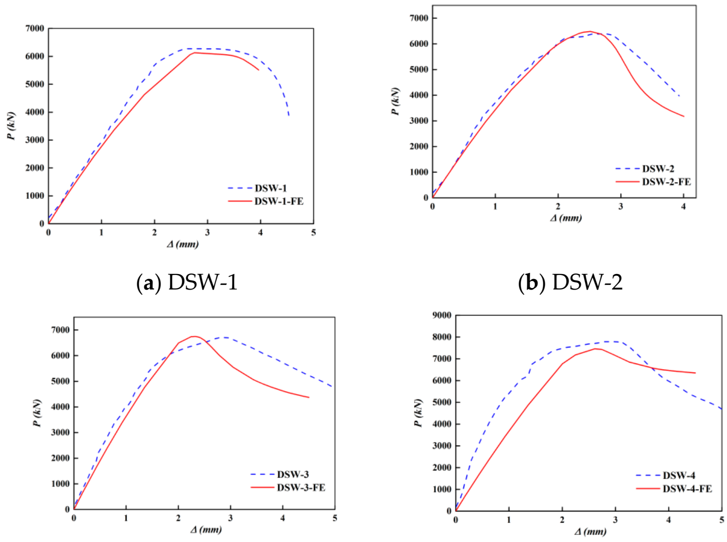

(**a**) DSW-1 (**b**) DSW-2

(**c**) DSW-3 (**d**) DSW-4

Figure 8. Experimental and numerical in-plane displacement curves (P-Δ curves) of SCS sandwich walls.

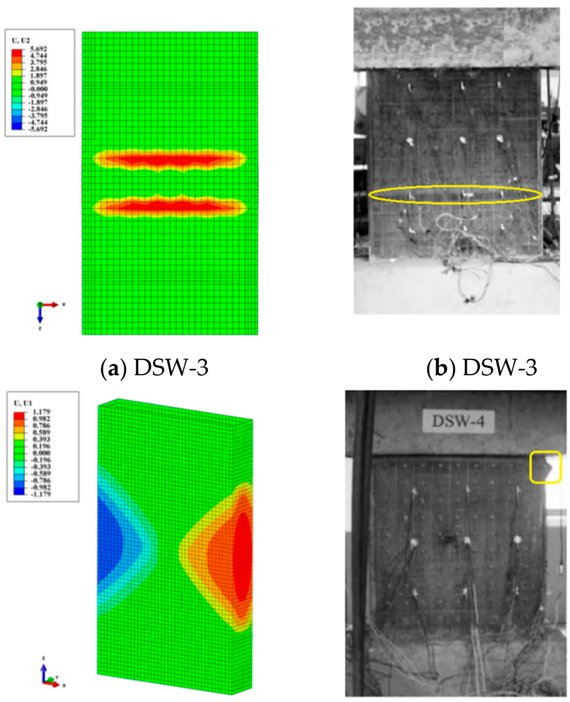

(**a**) DSW-3 (**b**) DSW-3

(**c**)DSW-4 (**d**) DSW-4

Figure 9. Comparisons of the failure modes between those from the FE simulations and the experimental tests.

Overall, the FE models can estimate the compressive behavior of the composite wall reasonably. Slight deviations of initial stiffness caused by the measurement method and the distribution of buckling caused by the uncertainty of initial imperfection of steel face plates can be accepted in the numerical analysis.

4. Numerical Simulation and Parametric Analysis

4.1. Failure Modes and Ultimate Resistance

The dimension, ultimate compressive resistances of FE models of the specimens are listed in Table 2.

Table 2. Dimension, ultimate compressive resistance, and ductility index of FE modeled specimens.

Specimen	Specimen Size							Enhancement	N_{FEM}	Δ_u	$\Delta_{0.85}$	DI
	H	b	t	t_c	t_s	t_r	s		(kN)	(mm)	(mm)	
SDC-REF	600	600	100	90	3	2	75	ss+sl	3398.1 ‘	1.126	1.620	1.438
SCS	600	600	100	94	3	0	75	/	3405.2	1.123	1.359	1.210
SDC-sleeve	600	600	100	90	3	2	75	sl	3325.9	1.059	1.367	1.291
SDC-sheet	600	600	100	90	3	2	75	ss	3243.8	1.068	1.516	1.419
SDC-no enh	600	600	100	90	3	2	75	/	3108.4	1.033	1.212	1.173
SDC-R1	600	600	100	92	3	1	75	ss+sl	3444.9	1.126	1.599	1.420
SDC-R3	600	600	100	88	3	3	75	ss+sl	3352.6	1.126	1.634	1.451
SDC-R5	600	600	100	84	3	5	75	ss+sl	3270.7	1.122	1.843	1.643
SDC-R8	600	600	100	78	3	8	75	ss+sl	3166.9	1.195	1.968	1.647
SDC-R10	600	600	100	74	3	10	75	ss+sl	3079.1	1.129	1.957	1.734
SDC-R15	600	600	100	64	3	15	75	ss+sl	2896.2	1.175	2.057	1.751
SDC-T4	600	600	100	88	4	2	75	ss+sl	3879.1	1.100	1.950	1.773
SDC-T5	600	600	100	86	5	2	75	ss+sl	4344.2	1.185	3.693	3.116
SDC-T6	600	600	100	84	6	2	75	ss+sl	4810.2	1.238	5.289	4.272
SDC-S100	600	600	100	90	3	2	100	ss+sl	3211.7	0.988	1.296	1.311
SDC-S150	600	600	100	90	3	2	150	ss+sl	2773.2	1.057	1.327	1.255
SDC-C100	600	600	110	100	3	2	75	ss+sl	3658.3	1.169	1.763	1.509
SDC-C110	600	600	120	110	3	2	75	ss+sl	3918.6	1.147	1.838	1.603
SDC-R5C100	600	600	110	94	3	5	75	ss+sl	3563.9	1.162	2.110	1.710
SDC-R5C110	600	600	120	104	3	5	75	ss+sl	3803.3	1.192	1.990	1.815
SDC-R5T4	600	600	100	82	4	5	75	ss+sl	3754.8	1.178	3.006	2.551
SDC-R5T5	600	600	100	80	5	5	75	ss+sl	4212.0	1.194	4.527	3.792
SDC-ss15	600	600	100	90	3	2	75	ss+sl	3364.2	1.1	1.434	1.315
SDC-ss35	600	600	100	90	3	2	75	ss+sl	3432.5	1.1	2.044	1.793
SDC-ss(sq)25	600	600	100	90	3	2	75	ss+sl	3409.9	1.1	1.768	1.571

*H = height of specimen; b = width of specimen; t = thinkness of specimen, t $= t_c + 2t_s + 2t_r$; t_c = thickness of concrete core; t_s = thickness of steel plate; t_r = thickness of rubber layer; s = binding bar spacing; N_{FEM} = failure load by FEM; SDC-REF= the reference specimen of SDC walls; ss = steel sheet, sl = sleeve; and DI = ductility index.

As shown in Figure 10, there are two main types of failure modes of the modeled SDC walls observed and the failure is defined as the compressive resistance of the wall decreased to 85% of its ultimate compressive resistance. The first type of failure is the high strain of concrete and local buckling of steel plates, as shown in Figure 10a. This type of failure is initially characterized by the high strain of the middle of concrete where the concrete suffers splitting and crushing along with the external steel plate yielding. Accordingly, the steel plate tends to buckle outward at the middle part, since the sectional stiffness degrades due to the cracking of the concrete core. The rubber layer is still bonded and deformed with the steel plate. All specimens except SDC-S150 fail in this type of mode.

The second type of failure mode represents a more severe buckling of outer steel plates, as shown in Figure 10b. This type of failure mode occurred in specimen SDC-S150. From Figure 10b, strip-shaped yield zones and a more severe buckling of steel plates can be observed, i.e., the maximum horizontal buckling displacement of steel plate in SDC-S150 is 6.71 mm which is 80% higher than that in SDC-REF with a value of 3.71mm. The rubber layer is also bonded and deformed with the steel plate. Besides, the highest value of concrete strain is 0.00137 which is lower than 0.00165 for the uniaxial ultimate compressive strain of the concrete. This means that no splitting failure in the concrete core is observed.

This type of failure takes place due to inadequate shear bond and insufficient shear connector design between the steel plates, the rubber layer, and the concrete.

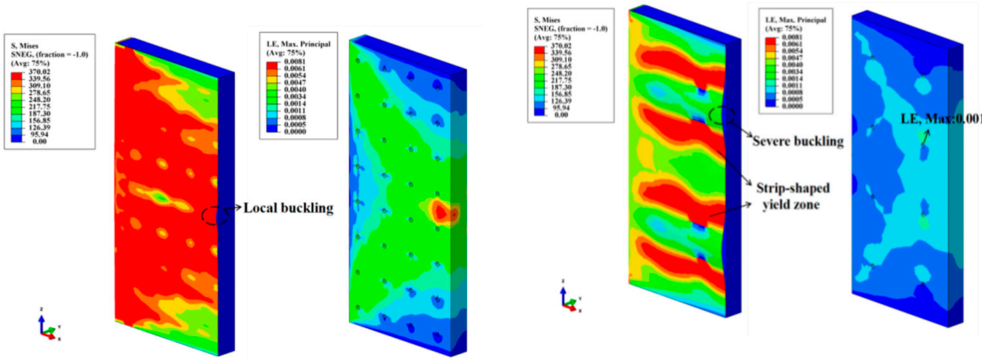

(**a**) The first type of failure mode (**b**) The second type of failure mode

Figure 10. Two failure modes of the SDC walls (deformation scale factor = 5.0).

4.2. Ductility Index

The ductility index (DI) represents the ability to undergo large plastic deformation without significant strength degradation. The DI equals to the displacements corresponding to 85% of the ultimate resistance during the recession stage, $\Delta_{85\%}$, to the displacement corresponding to ultimate resistance as follows:

$$\mathrm{DI} = \frac{\Delta_{85\%}}{\Delta_{\mathrm{U}}} \tag{9}$$

where DI denotes ductility index; and $\Delta_{85\%}$ and Δ_{U} are shown in Figure 1.

All the calculated DI ratios are given in Table 2.

4.3. Comparison of The SCS Wall and SDC Wall

Figure 11 shows the compression force versus in-plane displacement curves (P-Δ curves) of the SCS wall and SDC wall (the thickness of its rubber layer is 2 mm) with the same cross-section area in FEM. Three working stages are observed in both curves: Elastic stage, nonlinear stage, and recession stage. During the elastic stage (curve OA), the reaction forces of the composite walls linearly increase with the rising displacement and the two types of walls show similar initial stiffness. In the nonlinear stage (curve AB), nonlinear behaviors and similar ultimate compressive resistances can be seen in the two curves. In the recession stage (curve BD and BD´), the two types of walls show different reducing rates of the reaction forces. Compared with curve BC´, curve BC shows the reaction force of the SDC wall decreasing to its 85% peak load with more displacement which means the SDC wall is characterized with more ductility than the traditional SCS wall. This can be attributed to the rubber layer and reinforcement enhancements in the SDC wall.

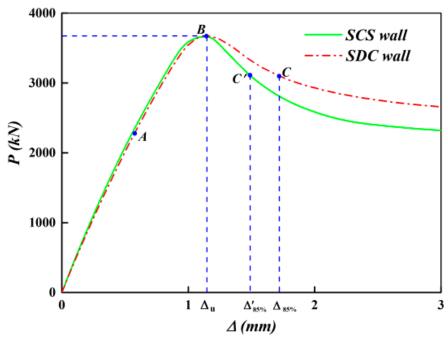

Figure 11. P-Δ curves of the SCS wall and SDC wall.

4.4. Discussions

4.4.1. Effect of the Damping Layer and the Reinforcement Enhancement

Figure 12 shows the compressive behavior of the SCS and SDC walls with different types of reinforcement enhancements. It can be observed that embedding rubber layers, steel sheets, and (or) sleeves in composite walls can significantly change their ultimate compressive resistance and ductility. Specifically, SDC-no enhan, the specimen without any reinforcement enhancements, shows the 9.6% decrease of ultimate compressive resistance, compared with the SCS wall. This is because: (i) the rubber layer fails to provide effective lateral confinement for the concrete core due to its low elasticity modulus and (ii) setting the damping interlayers causes the separation of concrete and steel plate as well as concrete and binding bars. The former one leads to the decrease in the confinement of steel plate on concrete directly, and the latter one results in the loss of embedment effect of binding bars on concrete and the decrease of the tensile resistance of the binding bars which can determine the magnitude of the confinement on concrete provided by the steel plate [3].

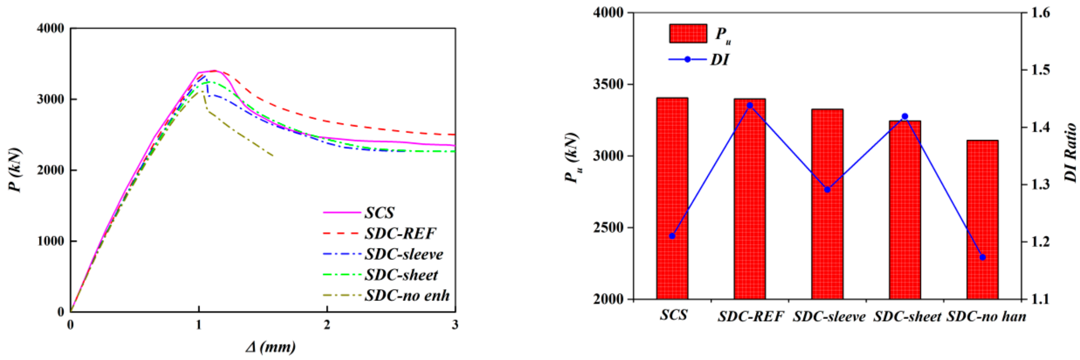

(**a**) The P-Δ curves (**b**) The P_u and DI Ratio

Figure 12. The compressive behavior of SCS wall and SDC walls with different enhancements.

To ensure sufficient lateral confinement, the composite walls with steel sheets and (or) sleeves are conducted. It can be found in Figure 12b that compared with the SCS wall, the walls with steel sheets (specimen SDC-sheet), sleeves (specimen SDC-sleeves), and both of them (specimen SDC-REF) show 5.0%, 2.4%, and 0.2% reduction of compressive capacity, respectively. This is because the steel sheets and sleeves improve not only the steel content of the composite wall but also the lateral confinement on the concrete core. Figure 13 shows the lateral Von-Mises stress (S22) contours of the concrete core of the five composite walls under the 85% ultimate compressive resistance (post-peak). In Figure 13e, the lateral stress (S22) of the concrete core of SDC-no enhan is marginal due to the lack of lateral confinement in spite of stress concentration induced by holes. Figure 13c shows higher S22 of concrete elements near steel sheets of SDC-sheet because of the lateral confinement on concrete core provided directly by steel sheets. Figure 13d shows a uniform and higher S22 of concrete element near sleeves of SDC-sleeve. This is because larger lateral expansion occurred in the concrete near the sleeves under compression due to the high elastic modulus of steel, which leads to higher reaction force on the concrete provided by the rubber layer and the steel plates. Moreover, it can be seen in Figure 13b that the concrete core of the SDC wall-REF is subjected to the largest lateral constraint even more than that of the SCS wall due to the combined action of steel sheets and sleeves. In such a case, the SDC walls have an equivalent ultimate compressive resistance of SCS walls which is essential for being used in high-rise buildings or special structures.

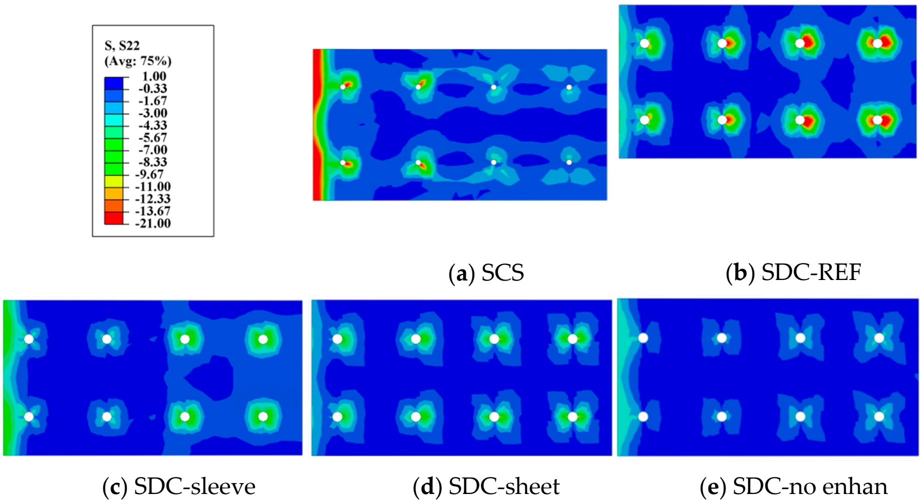

Figure 13. The lateral stress (S22) of the concrete core of SDC walls.

Figure 12b also shows that, compared with the SCS wall, a 0.3% decrease in the ductility of the SDC-no enhan while the SDC-steel sheet, SDC-sleeve, and SDC-REF show 14.7%, 6.3%, and 15.8% increases in the ductility, respectively. The decrease of ductility of SDC-no enhan is also because of the insufficient lateral restraint due to the separation of the concrete core and the steel plate caused by embedding the rubber layer. It is known that the longitudinal compression failure of concrete materials is caused by lateral tensile cracking. Compared with the concrete core of the SCS wall restrained by steel plates under two-axial compression, the concrete core of SDC-no enhan is subjected to lower confining stress. When the concrete core reaches the ultimate compressive load, the longitudinal crack expands rapidly and its low tensile deformation ability results in brittleness. On the other hand, the increase of ductility of the SDC-sheet, SDC-sleeve, and SDC-REF can be attributed to the (i) higher lateral confinement provided by steel sheets and (or) sleeves; and (ii) the rubber layer provides more deformation space of concrete core. Figure 14 shows the deformation of the three layers in the SDC wall. When the concrete core deforms laterally under compression, the outside rubber deforms longitudinally instead of laterally in the elastic (or hyperelastic) state due to the low elastic modulus and high ductility. This means the concrete in these specimens can undergo more deformation and consume more energy than concrete in the SCS wall. Meanwhile, the rubber layers also consume energy due to deformation.

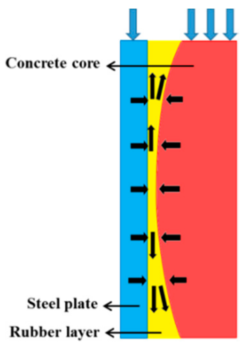

Figure 14. The deformation of three layers in the SDC wall.

4.4.2. Effect of Thickness of the Damping Layer

Figure 15 shows the influence of the thickness of the damping layer on the ultimate compressive resistance and DI ratios of SDC walls. Seven different thicknesses (t_r = 1, 2, 3, 5, 8, 10, and 15 mm) of damping layers were used in the parametric studies. It can be seen that increasing the thickness of the damping layer leads to a linear decrease of the ultimate compressive resistance of SDC walls. This is caused by the degressive lateral confinement on the concrete core provided by the steel plates due to the incremental thickness of the rubber layer and lessened interaction between concrete core and steel plate. Meanwhile, the ductility of the walls improves significantly as the damping layer becomes thicker. Specifically, augmenting the thickness of the damping layer from 0 to 2 mm and 5 mm, the DI ratio was increased by 18% and 35%, respectively. This is mainly because the thicker rubber layer which can provide more deformable space of concrete core contributed to more energy consumption and better ductility of the SDC wall. However, the increase of the DI ratio becomes steady for the thickness of the rubber layer more than 5 mm. This indicates that a thickness of 5mm is the threshold of lateral deformation of the concrete core for such SDC walls under compression loads when the walls failed. When the thickness of the rubber layer exceeds this threshold, the ductility of the wall resulted from the high ductility of the rubber marginally increases. Thus, in terms of ductility, the thickness of the rubber layer of SDC walls should not exceed 5 mm in the design phase. It is also worthwhile to mention that the SDC wall with a 2 mm rubber layer has the equivalent loading capacity of the SCS wall with the same cross-section area, which is fundamental to the bearing wall.

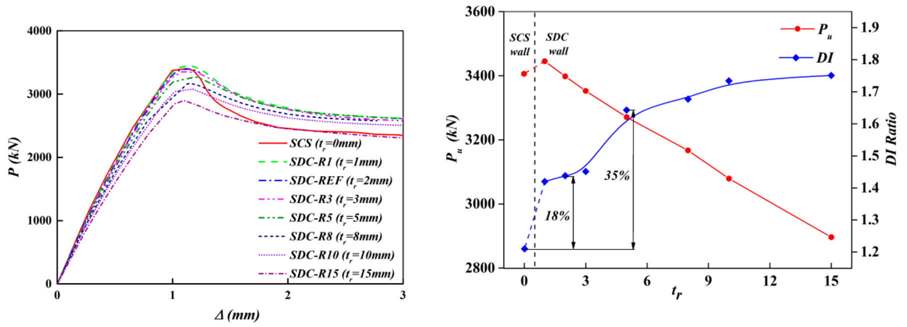

(**a**) The P-Δ curves (**b**) The P_u and DI Ratio

Figure 15. Influence of thickness of rubber layer on compressive resistance of SDC wall.

4.4.3. Effect of Thickness of the Concrete Core

Figure 16 shows the influence of the thickness of the concrete core on the compressive behavior of SDC walls with different thicknesses of rubber layers (t_r = 2 and 5 mm). The concrete core thicknesses of specimens are 90, 100, and 110 mm. It can be found that increasing the thickness of the concrete core increased the ultimate compressive resistance of SDC walls. Increasing the thickness of the concrete core from 90 mm to 100mm and 110 mm, the ultimate compressive resistance of walls with 2 (5) mm rubber layers is risen by 7.7% (9.0%) and 15.3% (16.3%), respectively. The increment can be attributed to the increase of the cross-sectional area of the concrete. It can also be seen that the DI ratio increases negligibly as the concrete becomes thicker, which means the thickness of the concrete core has less influence on the ductility of SDC walls.

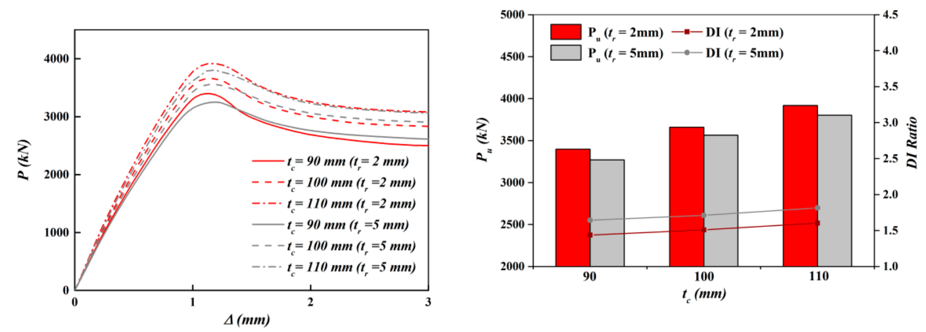

(**a**) The P-Δ curves (**b**) The P_u and DI Ratio

Figure 16. Influence of thickness of concrete on compressive resistance of SDC wall.

4.4.4. Effect of Thickness of Steel Plate

Figure 17 shows the influence of the thickness of the steel face plates on compressive resistance and ductility of SDC walls with two types of thicknesses of rubber layers (2 mm and 5 mm). It is found that the thickness of the steel face plate significantly influences the ultimate compressive resistance of the SDC wall. Increasing the thickness of the steel plate from 3mm to 4mm and 5mm, the ultimate compressive resistance of the SDC walls with 2 (5) mm rubber layers was increased by 14.2% (10.5%) and 27.8% (24%), respectively. This is because increasing the thickness of the steel face plates would contribute to (i) rising confinement on the concrete core, and (ii) increasing the buckling resistance and larger out-of-plane buckling stiffness of the steel plate [7].

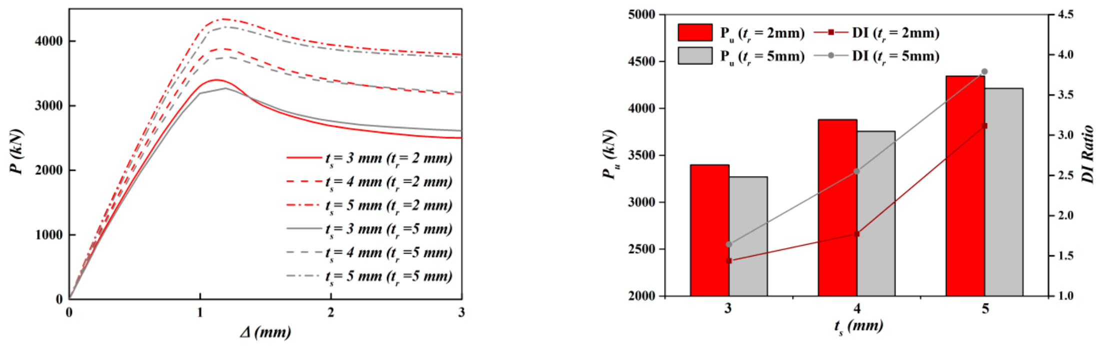

(**a**) The P-Δ curves (**b**) The P_u and DI Ratio

Figure 17. Influence of thickness of steel plates on compressive resistance of SDC wall.

Increasing the thickness of the steel face plate also resulted in a significant enhancement of the ductility of the SDC walls. As the thickness of the steel face plates increases from 3 mm to 4 mm and 5 mm, the DI ratios of the SDC walls with the 2mm (5 mm) rubber layer increase by 23.2% (55.3%) and 116.7% (130.8%). The increases are caused by the increased steel content of the cross-section. One interesting observation is that the influence of the plate thickness on the ductility of the SDC wall is more significant for the specimens with 5 mm rubber layers than the specimens with 2 mm rubber layers. This can be explained by that the concrete core with thicker steel plates can be more insensitive to the weakening effect of the rubber layer. Although the concrete core and steel plates are separated by the damping interlayer, the thicker steel plates still can provide relative effective lateral confinement on the concrete core.

4.4.5. Effect of Spacing of Binding Bars

The binding bar spacing for SDC-REF, SDC-S100, and SDC-S150 are 75, 100, and 150 mm, respectively, which leads to different plate slenderness ratios (s/t_s) of 25, 33, and 50. SDC-S150 is the specimen with partial composite design in which local buckling of steel plates occurs showing a brittle failure. Figure 10b illustrates the failure modes of SDC-S150, according to the LE contours, the buckling phenomenon is observed between two adjacent binding bars and no splitting failure occurs in the concrete core. This indicates insufficient connector design results in premature buckling of the steel plate that causes inferior use of the cross-sectional resistance of concrete and lower compressive resistance and ductility of the wall.

Figure 18 shows the influence of binding bar spacing on the ultimate compressive resistance and DI ratios of the SDC wall. It can be seen that the ultimate compressive resistance and ductility of the SDC wall decrease as the spacing of binding bar increases. Compared with SDC-REF, SDC-S1 and SDC-S2 exhibit a 5.8% and 22.5% decrease in the ultimate compressive resistance, respectively. Besides, the DI ratio is reduced by 9.7% and 14.5% from 1.44 to 1.31 and 1.26, respectively. These decrements in both ultimate compressive resistance and ductility are caused by lessened lateral constraint due to the insufficient shear connectors with wider spacing.

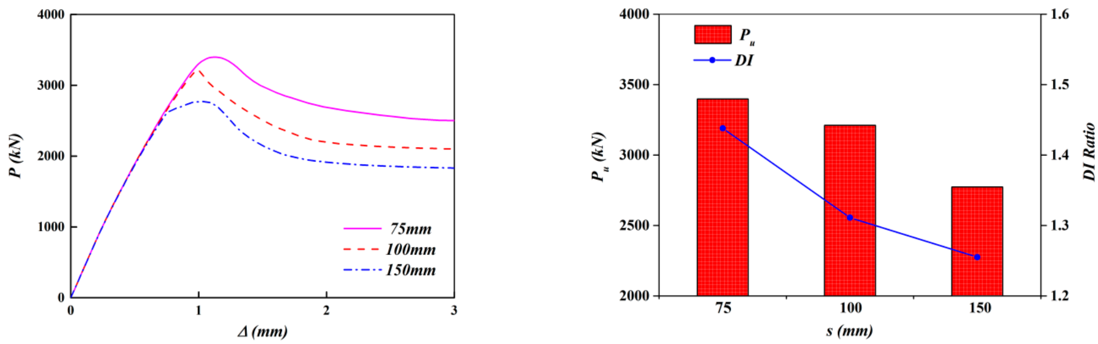

(**a**) The P-Δ curves (**b**) The P_u and DI Ratio

Figure 18. Influence of spacing of binding bars on compressive resistance of SDC wall.

Figure 19 shows the relation between plate slenderness ratio (s/t_s) and normalized compression resistance including the FE data of specimens SDC-S1 and SDC-S2. As can be seen, the increase in plate slenderness ratio could decrease the normalized compressive resistance. However, the normalized compressive resistance difference is within 10% with (s/t_s) ≤ 15. The normalized maximum compressive load resistances are reduced by about 30% and 40% when the plate slenderness ratio increases from 12.5 to 25 (s = 75 mm) and 50 (s = 150 mm), respectively.

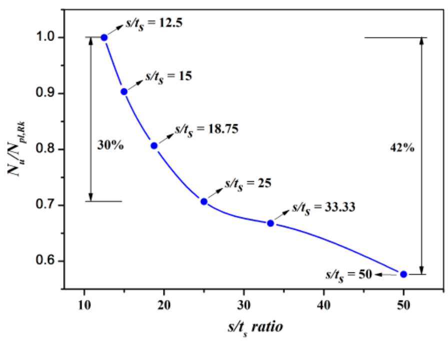

Figure 19. The relation between normalized strength and plate slenderness (s/ts).

4.4.6. Effect of the Diameter and Shape of Steel Sheets

Figure 20 shows the influence of the diameter and the shape of steel sheets on the ultimate compressive resistance and DI ratio of the SDC wall. It can be found that increasing the diameter leads to slight increases of the ultimate compressive resistance and initial stiffness. This is because the changes of the cross-sectional area of the steel sheets are marginal compared to the cross-sectional area of the wall.

However, it can be indicated that the diameter of steel sheets has an obvious influence on the ductility of SDC walls. The DI ratios are increased by 9.3% and 36.4% as the diameter increases from 15 mm to 25 mm and 35 mm. This can be explained that steel sheets can provide lateral restraint on the concrete core and thus inhibit the development of transverse cracks in the concrete after the concrete reaches the compressive strength. The steel sheet with a larger diameter can provide a larger area of constraints on the concrete.

It can also be found that changing the shape of steel sheets from circle (diameter = 25 mm) to square (side length = 25 mm), the ultimate compressive resistance and DI ratio increases moderately. This is because the increased area of steel sheets provides more confinement on the concrete core. However, compared to a circular sheet, when the wall is under pressure, the square sheet is more prone to undergo stress concentration at its corners and to scratch the rubber layer. Hence, considering the mechanical properties and durability of the structure, the circular steel sheet with a diameter of 25 mm is utilized in the SDC wall.

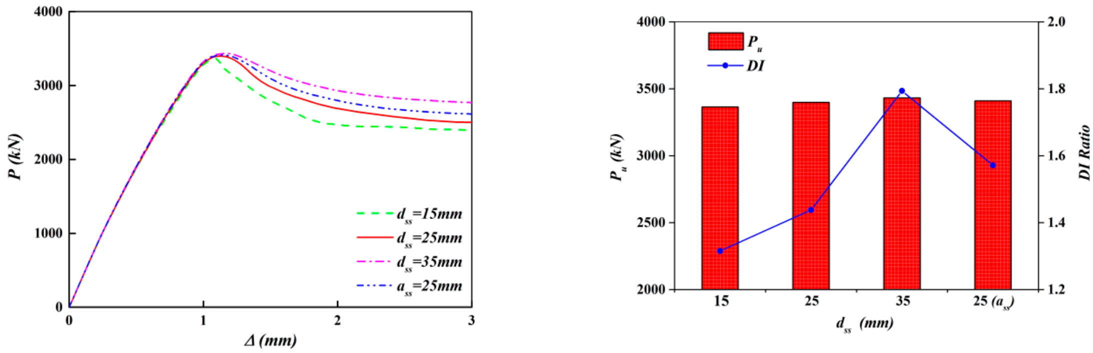

(**a**) The P-Δ curves (**b**) The P_u and DI Ratio

Figure 20. Influence of the diameter (side length) of steel sheets on compressive resistance of SDC wall.

5. Compressive Resistance of SDC Sandwich Wall

5.1. Code Method

Methods to calculate the compressive resistance of normal-sectioned composite columns under axial load are included in Eurocode 4 [46], AISC360-10 [47], and other references.

According to Eurocode 4, the compressive resistance of a composite cross-section should be calculated as the following;

$$P_u = f_{ya}A_a + 0.85f_cA_c + f_yA_s \tag{10}$$

where A_a and f_{ya} denote cross-sectional area and yield strength of reinforcement; A_s and f_{yd} denote the cross-sectional area and design; A_s and f_y denote cross-sectional area and yield strength of steel face plate.

In AISC 360-10, the compressive resistance of composite members is specified as the following,

$$P_u = P_{u0}\left(0.658^{P_{u0}/P_e}\right), \text{ when } P_{n0}/P_e \leq 2.25 \tag{11}$$

$$P_u = 0.877P_e, \text{ when } P_{n0}/P_e > 2.25 \tag{12}$$

where $P_u = f_yA_s + f_{ya}A_a + 0.85f_cA_c$; $P_e =$ elastic critical buckling load, and equal to $\pi^2(EI_{eff})/\left(KL^2\right)$; $K =$ effective length factor; $L =$ laterally unbraced length of the member.

Even though the confining effect of the out steel plate on the concrete is ignored in Equations (10) and (11), the two code methods still are found to over-predict the compressive resistance of the SCS sandwich wall [3] and SDC walls. The predictions are compared with the numerical results in Table 3. The average ratios of N_{FEM}/N_{EC4} and N_{FEM}/N_{AISC} are 0.953 and 0.975, respectively, with the same standard deviation of 0.045. This is because the criteria of codes were developed for composite columns and disregard the premature buckling of steel plates and incomplete material properties of concrete in composite walls. Furthermore, it can be observed from Figure 16 that the two codes obtain inferior predictions when the thickness of the rubber layer is higher than 5 mm, which means that the incomplete material properties of concrete are more influential, and it cannot be ignored in predictions of the SDC wall.

Table 3. Comparison of compressive resistance between calculated and numerical results.

Specimen	N_{FEM} (kN)	N_{EC4} (kN)	N_{AISC} (kN)	$N_{Equation(13)}$ (kN)	$N_{Equation(14)}$ (kN)	$N_{proposd}$ (kN)	N_{FEM}/N_{EC4}	N_{FEM}/N_{AISC}	$N_{FEM}/N_{Equation(13)}$	$N_{FEM}/N_{Equation(14)}$	$N_{FEM}/N_{proposed}$
CFSPD-R1	3445	3532	3446	2573	3201	3464	0.975	1.000	1.339	1.076	0.994
CFSPD-R2	3398	3520	3434	2528	3172	3414	0.965	0.989	1.344	1.071	0.995
CFSPD-R3	3353	3508	3422	2484	3143	3366	0.956	0.980	1.349	1.067	0.996
CFSPD-R4	3327	3496	3411	2440	3113	3320	0.952	0.975	1.363	1.069	1.002
CFSPD-R5	3271	3484	3399	2396	3084	3276	0.939	0.962	1.365	1.061	0.998
CFSPD-R8	3167	3449	3364	2264	2996	3153	0.918	0.942	1.399	1.057	1.004
CFSPD-R10	3079	3425	3340	2176	2937	3080	0.899	0.922	1.415	1.048	1.000
CFSPD-R15	2896	3366	3281	1955	2791	2927	0.861	0.883	1.481	1.038	0.989
CFSPD-T4	3879	3952	3865	2864	3604	3880	0.982	1.004	1.354	1.076	1.000
CFSPD-T5	4344	4384	4293	3238	4036	4346	0.991	1.012	1.342	1.076	1.000
CFSPD-T6	4810	4816	4720	3653	4468	4812	0.999	1.019	1.317	1.076	1.000
CFSPD-S100	3212	3405	3325	2245	3000	3216	0.943	0.966	1.430	1.071	0.999
CFSPD-S150	2773	3324	3247	2043	2412	3027	0.834	0.854	1.357	1.150	0.916
CFSPD-C100	3658	3700	3623	2749	3319	3582	0.989	1.010	1.331	1.102	1.021
CFSPD-C110	3919	3879	3810	2970	3465	3750	1.010	1.028	1.320	1.131	1.045
CFSPD-R5C100	3564	3657	3581	2617	3231	3423	0.975	0.995	1.362	1.103	1.041
CFSPD-R5C110	3803	3836	3767	2837	3377	3578	0.991	1.010	1.340	1.126	1.063
CFSPD-R5T4	3755	3916	3829	2729	3516	3739	0.959	0.981	1.376	1.068	1.004
CFSPD-R5T5	4212	4349	4258	3100	3948	4203	0.969	0.989	1.359	1.067	1.002
Mean							0.953	0.975	1.365	1.081	1.004
Std.dev							0.045	0.045	0.040	0.028	0.028

*N_{FEM} = failure load by FEM; N_{EC4} = predictions by Eurocode 4; N_{AISC} = predictions by AISC 360-10; $N_{Equation\ (13)}$ = predictions by Equation (13); $N_{Equation\ (14)}$ = predictions by Equation (14).

Methods for predicting the compressive resistance of concrete-filled tubular columns and SCS walls with binding bars are proposed in other references. The corresponding prediction models were also derived based on calibration with the numerical results, as given below,

$$N_u = \varnothing_1 f_y A_s + \varnothing_2 f_{ck} A_c \tag{13}$$

where $\varnothing_1 = \begin{cases} 0.898, R < 0.85 \\ 0.898R^{-0.7407}, R \geq 0.85 \end{cases}$ and $\varnothing_2 = 1.039R^{-0.0861}(7.3836\varsigma + 1.0588)$ [36].

$$N_u = \alpha_c f_c A_c + \sigma_{cr} A_s + f_{cy,2} A_{side} \tag{14}$$

$$\alpha_c = \begin{cases} 1, s \geq 100, \sigma_{cr} < f_y \\ \beta, s < 100, \sigma_{cr} < f_y \\ \beta\beta_2, \quad \sigma_{cr} = f_y \end{cases} \tag{15}$$

where $\beta = 0.8\left(\frac{150}{s}\right)^{0.23}$, $\beta_2 = \begin{cases} \min\left(1 + 8 \times 10^{-6} s\left(\frac{s_{cr}}{t} - \frac{s}{t}\right)^2, \ \frac{s+450}{500}\right), \beta < 1 \\ \max(1.2 - 0.01s/t, \ 1), \beta \geq 1 \end{cases}$, $s_{cr} = \pi\left(E_s/5.88/f_y\right)^{0.5} t$; α_c denotes the reduction factor of concrete considering the weakening effect caused by the ratio of the thickness of steel plates to the spacing of binding bars and initial imperfection of steel face plates; σ_{cr} denotes the buckling stress of steel face plates; $f_{y,2}$ and A_{side} denote the yield strength and cross-sectional area of steel side plates; β denotes the reduction factor of concrete considering that steel plates fail to provide post-buckling strength after buckling caused by the large spacing of binding bars and initial imperfection of steel plates; β_2 denotes the enhancement factor of concrete considering the confinement provided by external steel plates [44].

Table 3 compares the compressive resistance obtained by the other researchers' models and the numerical results. Figure 21 plots the numerical results and predictions by Equations (13) and (14). It is observed that Equation (13) underestimates the compressive resistance of the SDC sandwich wall with binding bars noticeably. This is because the width-thickness ratio parameter R, the only parameter related to the sectional characteristics, leaves out the effect of binding bars on the postponement of the buckling of the steel plate. This disregard cannot be accepted in SCS and SDC walls due to the smaller aspect ratio (< 2.0) of composite walls compared to CFT columns with larger aspect ratios (> 4.5). It also can be found that Equation (14) underestimates the compressive resistance of the SDC sandwich wall, as this method could not take the steel sheets and sleeves into consideration. These reinforcement enhancements indeed improve the compression resistance of SDC walls because they improve the steel content and confinement effect on the concrete. Based on the above discussion, a new formula shall be developed to predict the compressive resistance of the SDC composite walls.

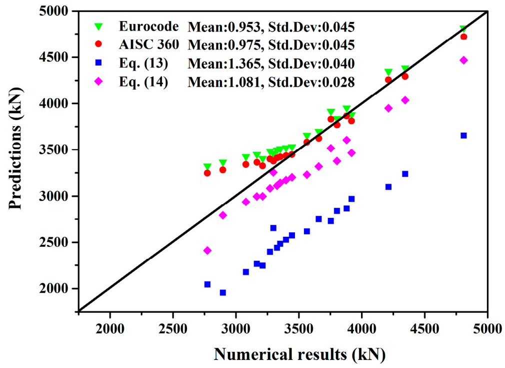

Figure 21. Comparison of numerical results with predicted results.

5.2. Theoretical Method

For simplification, the following methods and assumptions may be applied:

(1) Based on the strength superposition method, the compressive resistance of the SDC composite wall consists of four parts: The compressive resistance of the concrete core, steel plates, reinforcement enhancements, and rubber layer.

$$N_u = N_c + N_s + N_{rein} + N_{rub} \tag{16}$$

(2) The compressive resistance of the rubber layer during the compression of the SDC wall can be calculated as follows:

$$N_{rub} = \sigma_{rub} A_{rub} = E_{rub} \varepsilon_{rub} A_{rub} \tag{17}$$

where σ_{rub}, ε_{rub}, and E_{rub} denote the stress, strain, and elastic modulus of the rubber layer.

Since the elastic modulus of rubber (7.84 MPa) is far less than that of concrete (3.35×10^4 MPa) and steel (2×10^5 MPa), N_{rub} is ignored in Equation (16). And Equation (16) becomes the following:

$$N_u = N_c + N_s + N_{rein} \tag{18}$$

(3) The effect of binding bars can be considered in the calculation of compressive resistance of the concrete core instead of reinforcement enhancements. And the influence of steel sheets and sleeves can be taken into consideration by the equivalent compressive resistance. In terms of binding bars, the confining influence of them on the concrete core is ignored in both AISC 360 and Eurocode 4 in order to improve safety reserves of the SCS composite wall. However, Yan [7] proposed that all the steel across the concrete failure plane can be assumed to provide confinement. The confinement stress σ_c was defined as equivalent stress distributed over the corresponding area on average, which can be expressed by

$$\sigma_c = \frac{nT}{WH} \tag{19}$$

where σ_c denotes the confinement stress of concrete; n denotes the number of connectors in a composite structure; W and H denote the width and height of the wall; T denotes the tensile resistance of connectors. Therefore,

$$\sigma_c = \frac{T}{s^2} \tag{20}$$

where s denotes the spacing between the neighboring connectors.

Furthermore, Wei [45] also proposed a formula to predict the confinement effect on the concrete of binding bars, as given in Equation (15). Given the above methods, the effect of binding bars in the SDC wall is considered in the compressive resistance of the concrete, as shown in Equations (15) and (27). However, steel sheets and sleeves, not only provide confinement on concrete but also provide compressive resistance directly. To get conservative prediction results, only the equivalent compressive resistance of steel sheets and sleeves are considered and the N_{rein} can be calculated by:

$$N_{rein} = N_{sheet} + N_{sleeve} = f_{y,3}A_{sheet} + f_{y,4}A_{sleeve} \tag{21}$$

$$A_{sheet} = n\frac{\pi r_{sheet}^2 t_{sheet}}{S} \tag{22}$$

$$A_{sleeve} = 2n\frac{\pi\left(r_{sleeve,2}^2 - r_{sleeve,1}^2\right)\left(t - 2t_{sp} - 2t_{sheet}\right)}{S} \tag{23}$$

where A_{sheet} and A_{sleeve} denote the equivalent cross-sectional area of the steel sheet and sleeve; r_{sheet} and t_{sheet} denote the radius and thickness of the steel sheet; and $r_{sleeve,1}$ and $r_{sleeve,2}$ denote the inner and outer radius of the sleeve

(4) The compressive resistance of steel plates can be calculated by adding the resistance of steel face plate and steel side plate:

$$N_s = \sigma_{cr}A_{surf} + f_{y,2}A_{side} \tag{24}$$

According to the suggestion of Akiyama [48], the yield stress of steel face plate can be calculated as follows:

$$\sigma_{cr} = \frac{\pi^2 E_s}{12\mu^2 (B/t)^2} \tag{25}$$

where E_s denotes the elastic modulus of the steel; μ denotes the effective length coefficient, and its value can be determined as 0.7 for safety reserves.

To demonstrate Equation (25) and investigate the effect of the plate slenderness ratio on buckling performance of SCS wall, buckling analysis and ultimate stress state analysis was carried out by Wei [45] and the following formula was proposed to compute the buckling stress of steel face plates:

$$\sigma_{cr} = \begin{cases} f_y, & s/t_s \le \pi\sqrt{E_s/(5.88 f_y)} \\ \frac{\pi^2 E_s}{5.88(s/t_s)}, & s/t_s > \pi\sqrt{E_s/(5.88 f_y)} \end{cases} \tag{26}$$

As can be seen in FE model, although the boundary conditions of steel face plates in SCS wall and SDC wall are not the same due to inner rubber layer and steel sheets, the local buckling modes of the steel face plates in these two types of composite walls are similar: The steel face plates are restrained and forced by inner concrete core and steel sheets, which can be seen as rigid media, to form away from the concrete [36]. Thus, Equation (26) can be utilized for calculating the buckling stress of steel face plates.

(5) The compressive resistance of concrete core can be calculated as follows:

$$N_c = \alpha_c f_c A_c \tag{27}$$

where α_c denotes the reduction factor of concrete considering the weakening effect caused by the ratio of the thickness of steel plates to the spacing of binding bars and rubber layer;

In the case of the SCS wall, α_c can be determined by the β and β_2, expressed as Equation (15); However, in terms of the SDC wall, the confinement on concrete provided by external steel plates is modest due to the rubber layer sandwiched between them, which means that β_2 can be removed. Instead, lateral cracks in the concrete core expand more easily because of the lack of restraint of bilateral steel plates, which leads to reduced compressive resistance of composite walls. This reduction is determined by the relationship of thicknesses of rubber layer, steel face plates, and concrete core. According to the numerical results, t_r and t_{sp} are more influential towards the reduction than t_c. In this paper, SDC walls with 100-mm-width sections are mainly investigated and the t_c can be seen as the function of the t_r and t_{sp}:

$$t_c = 100 - t_r - t_{sp} \tag{28}$$

Thus, γ was proposed as the reduction factor of concrete considering the weakening effect caused by the rubber layer. Based on the regression of FEM as shown in Figure 22, it is given as:

$$\gamma = 0.9836 - 0.03027 t_r + 0.02569 t_{sp} \tag{29}$$

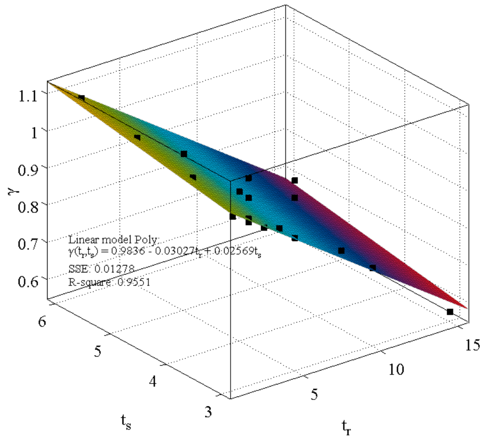

Figure 22. The γ relationship based on the regression method.

And the calculation of α_c in SDC wall becomes as the following:

$$\alpha_c = \begin{cases} 1 & B \geq 100, \sigma_{cr} < f_y \\ \beta & B < 100, \sigma_{cr} < f_y \\ \beta\gamma & \sigma_{cr} = f_y \end{cases} \tag{30}$$

5.3. Validations

The scatter plot between the numerical results and predictions by the proposed methods is depicted in Figure 23. It can be found that the proposed theoretical models can predict the ultimate compressive resistances of the SDC wall accurately, especially for walls with different thicknesses of rubber layers. The average ratio of numerical results to prediction $N_{FEM}/N_{proposed}$ is 1.004, with a standard deviation of 0.04. Compared with the code equations and other methods, the accuracy and scatter of the predictions on compressive resistance of SDS walls are improved in the proposed theoretical models, as the new methods take into account the weakening effect on concrete caused by the rubber layer and compressive resistance provided by enhancement reinforcements.

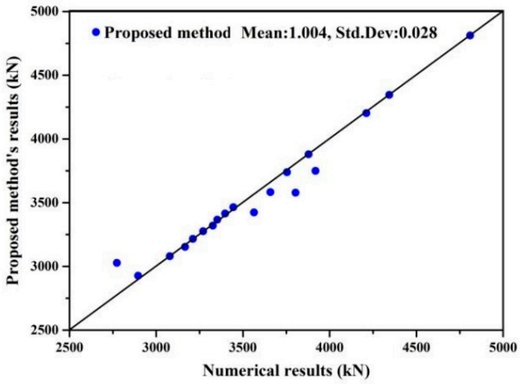

Figure 23. Comparison between numerical results and predictions by proposed methods.

5.4. Design Method to Predict Compressive Resistance of SDC Sandwich Wall

Step I: Using Equation (24) to calculate the compressive resistance of the steel plates, in which the buckling stress of steel face plate σ_{cr} considering the influence of plate slenderness ratio of the composite walls should be determined by Equation (26);

Step II: Using Equation (27) to calculate the compressive resistance of the concrete core, in which the concrete strength reduction factor α_c considering the weakening effect of the rubber layer, the large spacing of binding bars and initial imperfection of steel plates can be determined by Equations (29) and (30);

Step III: Using Equations (21)–(23), determine the equivalent compressive resistance of reinforcement enhancements;

Step IV: Determine the compressive resistance of the SDC sandwich walls using Equation (16) or (18).

6. Conclusions

This paper firstly introduced the rubber layer into the SCS composite wall and proposed the SDC wall to optimize the performance of various aspects of this versatile composite wall, including energy absorption, anti-explosion, and impact resistance. A novel connection technology, binding bar working with reinforcement enhancements (steel sheets and sleeves) was developed to compensate for the weakening effect of the rubber layer on the concrete core and to construct the SDC wall. This connection technology along with the introduction of rubber is utilized to allow the SDC wall characterized by the function of energy dissipation and comparable compressive bearing capacity with the SCS wall. A validated FE model was established to simulate the compressive performance of the SDC composite walls. An extensive parametric study was also carried out to optimize the design of the SDC walls. Finally, the bearing capacity formula is proposed to predict the compressive resistance of the SDC composite wall. Based on the numerical results, the following conclusions can be drawn:

(1) The numerical results proved that compared with the SCS wall, the SDC wall is characterized by comparable ultimate compressive resistance and better ductility. The increase in ductility can be attributed to the cooperation between the embedding rubber layer and reinforcement enhancements. In particular, only embedding the rubber layer in the composite wall failed to increase the ductility. The steel sheets and sleeves provided confinement on concrete core and thus improved the compressive resistance and ductility of the composite wall.

(2) From the parametric study, it was found that increasing the thickness of the damping layer can increase the ductility significantly but decrease the ultimate compressive resistance of the SDC wall. When the thickness of the rubber layer was around 2 mm, the SDC wall had a similar compressive bearing capacity of the SCS wall; when the thickness was more than 5 mm, the improving tendency of ductility of the SDC wall became slight.

(3) It was observed from the parametric study that (a) increasing both of the thickness of the concrete core and steel plate can offer higher compressive resistance of the SCD wall. However, in terms

of DI ratio, the thickness of the concrete core had less influence while the thickness of steel plates can improve it significantly; (b) increase of the spacing of the binding bars and plate slenderness of the SDC wall can reduce the compressive resistance and the DI ratio; and (c) the diameter of steel sheets has an obvious influence on the ductility of SDC walls.

(4) Theoretical models were developed to predict the ultimate compressive resistance of SDC composite walls. The developed models proposed a regression method to determine the weakening effect of the rubber layer on the concrete core and considered reinforcement enhancements by using an equivalent compressive resistance. The proposed design approach was accurately validated against the numerical results.

In this paper, compressive behaviors of SDC composite walls with specified cross-sections were investigated numerically and theoretically. The proposed concepts, models developed, and the results obtained are expected to provide meaningful guidance in the design of other composite walls with similar structural characteristics. Further theoretical and experimental studies are needed to cover an extensive range of SDC composite walls under other loading cases.

Author Contributions: L.Z. provided the conceptual design of the novel composite wall; L.Z. and D.A. conceived and designed the FE models; C.Z. and D.A. analyzed the data; C.Z. and D.A. wrote the paper.

Acknowledgments: The research is financially supported by the National Natural Science Foundation of China (Grant No. 51708318, 51678322), The International Postdoctoral Exchange Fellowship Program (Grant No. 20190015),Ministry of Science and Technology of China (Grant No. 2017YFC0703603), the Taishan Scholar Priority Discipline Talent Group program funded by the Shandong Province, the Cooperative Innovation Center of Engineering Construction and Safety in Shandong Blue Economic Zone scheme funded by the Shandong Province and the first-class discipline project funded by the Education Department of Shandong Province.

Conflicts of Interest: The authors declare no conflict of interest.

References

1. Oduyemi, T.O.S.; Wright, H.D. An experimental investigation into the behaviour of double skin sandwich beams. *J. Constr. Steel Res.* **1989**, *14*, 197–220. [CrossRef]
2. Liew, J.Y.R.; Sohel, K.M.A. Lightweight steel-concrete-steel sandwich system with J-hook connectors. *Eng. Struct.* **2009**, *31*, 1166–1178. [CrossRef]
3. Huang, Z.Y.; Liew, J.Y.R. Compressive resistance of steel-concrete-steel sandwich composite walls with J-hook connectors. *J. Constr. Steel Res.* **2016**, *124*, 142–162. [CrossRef]
4. Guo, Y.T.; Tao, M.X.; Nie, X.; Qiu, S.Y.; Tang, L.; Fan, J.S. Experimental and Theoretical Studies on the Shear Resistance of Steel-Concrete-Steel Composite Structures with Bidirectional Steel Webs. *J. Struct. Eng.* **2018**, *144*. [CrossRef]
5. Zhu, L.M.; Zhang, C.W.; Guan, X.M.; Uy, B.; Sun, L.; Wang, B.L. The multi-axial strength performance of composite structural B-C-W members subjected to shear forces. *Steel Compos. Struct.* **2018**, *27*, 75–87.
6. Zhang, C.; Gholipour, G.; Mousavi, A.A. Nonlinear dynamic behavior of simply-supported RC beams subjected to combined impact-blast loading. *Eng. Struct.* **2019**, *181*, 124–142. [CrossRef]
7. Yan, J.B.; Wang, X.T.; Wang, T. Compressive behaviour of normal weight concrete confined by the steel face plates in SCS sandwich wall. *Constr. Build. Mater.* **2018**, *171*, 437–454. [CrossRef]
8. Yan, J.B.; Liew, J.Y.R.; Zhang, M.H. Tensile resistance of J-hook connectors used in Steel-Concrete-Steel sandwich structure. *J. Constr. Steel Res.* **2014**, *100*, 146–162. [CrossRef]
9. Yan, J.B.; Liu, X.M.; Liew, J.Y.R.; Qian, X.D.; Zhang, M.H. Steel-concrete-steel sandwich system in Arctic offshore structure: Materials, experiments, and design. *Mater. Des.* **2016**, *91*, 111–121. [CrossRef]
10. Leng, Y.B.; Song, X.B. Shear strength of steel-concrete-steel sandwich deep beams: A simplified approach. *Adv. Struct. Eng.* **2019**, *22*, 42–53. [CrossRef]
11. Kristensen, R.F.; Nielsen, K.L.; Mikkelsen, L.P. Numerical studies of shear damped composite beams using a constrained damping layer. *Compos. Struct.* **2008**, *83*, 304–311. [CrossRef]
12. Montemurro, M.; Koutsawa, Y.; Belouettar, S.; Vincenti, A.; Vannucci, P. Design of damping properties of hybrid laminates through a global optimisation strategy. *Compos. Struct.* **2012**, *94*, 3309–3320. [CrossRef]

13. Yang, J.S.; Xiong, J.; Ma, L.; Wang, B.; Zhang, G.Q.; Wu, L.Z. Vibration and damping characteristics of hybrid carbon fiber composite pyramidal truss sandwich panels with viscoelastic layers. *Compos. Struct.* **2013**, *106*, 570–580. [CrossRef]
14. Yim, J.H.; Cho, S.Y.; Seo, Y.J.; Jang, B.Z. A study on material damping of 0° laminated composite sandwich cantilever beams with a viscoelastic layer. *Compos. Struct.* **2003**, *60*, 367–374. [CrossRef]
15. Wang, H.J.; Chen, L.W. Vibration and damping analysis of annular plates with constrained damping layer treatments. *J. Sound Vib.* **2003**, *264*, 893–910. [CrossRef]
16. Kumar, K.R.; Ganesan, N. Vibration and damping studies on a hollow sandwich box column with a viscoelastic/electrorheological/magnetorheological fliud core layer by the finite element method. *Int. J. Struct. Stab. Dyn.* **2008**, *8*, 531–546. [CrossRef]
17. Ramkumar, K.; Ganesan, N. Vibration and damping of composite sandwich box column with viscoelastic/electrorheological fluid core and performance comparison. *Mater. Des.* **2009**, *30*, 2981–2994. [CrossRef]
18. Xu, H.B.; Zhang, C.W.; Li, H.; Ou, J.P. Real-time hybrid simulation approach for performance validation of structural active control systems: a linear motor actuator based active mass driver case study. *Struct. Control Health Monit.* **2014**, *21*, 574–589. [CrossRef]
19. Fu, W.Q.; Zhang, C.W.; Sun, L.; Askari, M.; Samali, B.; Chung, K.L.; Sharafi, P. Experimental investigation of a base isolation system incorporating mr dampers with the high-order single step control algorithm. *Appl. Sci.* **2017**, *7*, 344. [CrossRef]
20. Zhang, C.; Wang, H. Swing Vibration Control of Suspended Structure Using Active Rotary Inertia Driver System: Parametric Analysis and Experimental Verification. *Appl. Sci.* **2019**, *9*, 3144. [CrossRef]
21. Meftah, S.A.; Daya, E.; Tounsi, A. Finite element modelling of sandwich box column with viscoelastic layer for passive vibrations control under seismic loading. *Thin-Walled Struct.* **2010**, *51*, 174–185. [CrossRef]
22. Li, G.; Liu, W.F.; Chen, G.L.; Ren, F. Experimental on Seismic Performance of Reinforced Concrete Columns Strengthened with Bonded Rubber Plate. *J. Civ. Eng. Manag.* **2018**, *35*, 130–136. (In Chinese)
23. Kim, J.K.; Mackay, D.B.; Mai, Y.W. Drop-weight impact damage tolerance of CFRP with rubber-modified epoxy matrix. *Composites* **1993**, *24*, 485–494. [CrossRef]
24. Ozturk, A.; Kaynak, C.; Tincer, T. Effects of liquid rubber modification on the behaviour of epoxy resin. *Eur. Polym. J.* **2001**, *37*, 2353–2363. [CrossRef]
25. Sarlin, E.; Liu, Y.; Vippola, M.; Zogg, M.; Ermanni, P.; Vuorinen, J.; Lepisto, T. Vibration damping properties of steel/rubber/composite hybrid structures. *Compos. Struct.* **2012**, *94*, 3327–3335. [CrossRef]
26. Sarlin, E.; Apostol, M.; Lindroos, M.; Kuokkala, V.T.; Vuorinen, J.; Lepisto, T.; Vippola, M. Impact properties of novel corrosion resistant hybrid structures. *Compos. Struct.* **2014**, *108*, 886–893. [CrossRef]
27. During, D.; Weiss, L.; Stefaniak, D.; Jordan, N.; Huhne, C. Low-velocity impact response of composite laminates with steel and elastomer protective layer. *Compos. Struct.* **2015**, *134*, 18–26. [CrossRef]
28. Davies, G.A.O.; Hitchings, D.; Zhou, G. Impact damage and residual strengths of woven fabric glass/polyester laminates. *Compos. Part A* **1996**, *27*, 1147–1156. [CrossRef]
29. Xu, L.R.; Rosakis, A.J. Impact failure characteristics in sandwich structures Part I: Basic failure mode selection. *Int. J. Solids Struct.* **2002**, *39*, 4215–4235. [CrossRef]
30. Wright, H.D. The axial load behaviour of composite walling. *J. Constr. Steel Res.* **1998**, *45*, 353–375. [CrossRef]
31. Liu, Y.B.; Yang, Q.N.; Liu, J.B.; Liao, Y.X. Experimental research on axial compressive behaviour of shear wall with double steel plates and filled concrete. *J. Sichuan Univ. (Eng. Sci. Ed.)* **2016**, *48*, 83–90.
32. Huang, Z.Y.; Liew, J.Y.R. Structural behaviour of steel-concrete-steel sandwich composite wall subjected to compression and end moment. *Thin-Walled Struct.* **2016**, *98*, 592–606. [CrossRef]
33. Huang, Z.Y.; Liew, J.Y.R. Numerical studies of steel-concrete-steel sandwich walls with J-hook connectors subjected to axial loads. *Steel Compos. Struct.* **2016**, *21*, 461–477. [CrossRef]
34. Yan, J.B.; Zhang, W. Numerical analysis on steel-concrete-steel sandwich plates by damage plasticity model: From materials to structures. *Constr. Build. Mater.* **2017**, *149*, 801–815. [CrossRef]
35. Sener, K.C.; Varma, A.H. Steel-plate composite walls: Experimental database and design for out-of-plane shear. *J. Constr. Steel Res.* **2014**, *100*, 197–210. [CrossRef]
36. Cai, J.; He, Z.Q. Axial load behaviour of square CFT stub column with binding bars. *J. Constr. Steel Res.* **2006**, *62*, 472–483. [CrossRef]
37. Cai, J.; Long, Y.L. Local buckling of steel plates in rectangular CFT columns with binding bars. *J. Constr. Steel Res.* **2009**, *65*, 965–972. [CrossRef]

38. Eom, T.S.; Park, H.G.; Lee, C.H.; Kim, J.H.; Chang, I.H. Behavior of Double Skin Composite Wall Subjected to In-Plane Cyclic Loading. *J. Struct. Eng.* **2009**, *135*, 1239–1249. [CrossRef]
39. Liu, H.; Cai, J.; Yang, C.; Chen, Q.; Zuo, Z. Experimental study on seismic behavior of composite shear wall with double steel plates and infill concrete with binding bars. *J. Build. Struct.* **2013**, *34*, 84–92. (In Chinese)
40. Zhu, L.; Zhou, D.; He, M. Experimental research on seismic behavior of composite concreteand steel plate shear walls with binding bars. *J. Build. Struct.* **2013**, *34*, 93–102. (In Chinese)
41. ABAQUS. *ABAQUS Standard User's Manual*, version 6.12. Providence; Dassault Systemes Corp: Johnston, RI, USA, 2012.
42. GB 50010-2010. *Code for Design of Concrete Structures*; China Stamdards Press: Beijing, China, 2010.
43. Lee, J.; Fenves, G.L. A Plastic-damage model for cyclic loading of concrete structures. *J. Eng. Mech.* **1989**, *124*, 892–900. [CrossRef]
44. Kim, B.; Lee, S.B.; Lee, J.; Cho, S.; Park, H.; Yeom, S.; Park, S.H. A Comparison Among Neo-Hookean Model, Mooney-Rivlin Model, and Ogden Model for Chloroprene Rubber. *Int. J. Precis. Eng. Manuf.* **2012**, *13*, 759–764. [CrossRef]
45. Wei, F.-F.; Zheng, Z.-J.; Yu, J.; Wang, Y.-Q. Computational method for axial compression capacity of double steel-concrete composite shear walls with consideration of buckling. *Eng. Mech.* **2019**, *36*, 154–164. (In Chinese)
46. BS EN 1994-1. *Eurocode 4: Design of Composite Steel and Concrete Structures: Part 1.1 General Rules and Rules for Buildings*; British Standards Institution: London, UK, 1999.
47. AISC. *ANSI/AISC 360-10, Specifification for Structural Steel Buildings*; American Institute of Steel Construction: Chicago, IL, USA, 2010.
48. Akiyama, H.; Sekimoto, H.; Fukihara, M.; Nakanishi, K.; Hara, K. A compression and shear loading test of concrete filled steel bearing wall. In Proceedings of the Transaction of the 11th International Conference on Structural Mechanics in Reactor Technology, Tokyo, Japan, 18–23 August 1991; International Association for Structural Mechanics in Reactor Technology: Tokyo, Japan, 1991; pp. 323–328.